

Mechanical Enhancement of Fractured Laminated Glass considering Fragment Overlaps and Temperatures

Dongdong Xie ^{a,b}, Jian Yang ^{a,b,*}, Xing-er Wang ^{a,b}, Xianfang Jiang ^c, Gang Li ^c

- a State Key Laboratory of Ocean Engineering, Shanghai Jiao Tong University, Shanghai 200240, PR China, hxqiay@sjtu.edu.cn
- b Shanghai Key Laboratory for Digital Maintenance of Buildings and Infrastructure, School of Ocean and Civil Engineering, Shanghai Jiao Tong University, Shanghai 200240, PR China
- c Henan Zhongbo Glass Co., LTD, Zhoukou, Henan, 466000, PR China

Abstract

The post-fracture performance of laminated glass is becoming a significant focus due to the growing breakage incidents of tempered glass and its long-term replacement. However, the influence of tension stiffening due to the adhesion of glass fragments to polymeric interlayers, one of the main factors affecting the structural capacity of the post-fracture laminated glass, is still unclear, especially when considering different fragment overlaps and temperatures. In this work, two types of uniaxial tensile tests with predefined cracks, including the multiple through-cracked tensile (MTCT) and the multiple offset-cracked tensile (MOCT), were conducted at 20, 50, and 80°C. Both PVB and SG were considered. Additionally, the influence of the overlap length of offset fragments and initial delamination on tension stiffening was investigated based on finite element models. The results show that the mechanical properties of the composite materials, which correspond to a local response in the post-fracture laminated glass, are strongly dependent on the fragment overlap, temperature, and interfacial delamination. Moreover, the influence of the fragment overlap on the mechanical enhancement becomes pronounced even at high temperatures, which should be taken into account for the evaluation of the post-fracture performance of laminated glass.

Keywords

Laminated Glass, Fragment Overlap, Temperature, Tension Stiffening, Delamination

Article Information

- Digital Object Identifier (DOI): [10.47982/cgc.9.493](https://doi.org/10.47982/cgc.9.493)
- Published by [Challenging Glass](#), on behalf of the author(s), at [Stichting OpenAccess](#).
- Published as part of the peer-reviewed [Challenging Glass Conference Proceedings](#), Volume 9, June 2024, [10.47982/cgc.9](https://doi.org/10.47982/cgc.9)
- Editors: Christian Louter, Freek Bos & Jan Belis
- This work is licensed under a [Creative Commons Attribution 4.0 International](#) (CC BY 4.0) license.
- Copyright © 2024 with the author(s)

1. Introduction

Laminated glass has been a promising structural component due to its transparency and safety. The design codes of glass structure are also constantly being improved with structural glass developing. The limit states of glass structure have been extended, including Serviceability Limit State (SLS), Ultimate Limit State (ULS), Fracture Limit State (FLS), and Post Fracture Limit State (PFLS) in CEN/TS 19100 (Feldmann et al., 2023) and SIA 2057 (Thomas et al., 2023). The post-fracture stage is emphasized for ensuring fractured glass components maintaining residual strength and stiffness in a required period of countermeasures or replacement. However, the verification in the PFLS is currently time-consuming and laborious based on fine numerical models (Wang et al., 2021) and bending experiments (Biolzi and Simoncelli, 2022). Limited researches about analytical model in PFLS could be found (Galuppi et al., 2013; Galuppi and Royer-Carfagni, 2016; D'Ambrosio et al., 2019), where homogenized models were developed for revising the interlayer stiffness due to the tension stiffening (TS) effect. The TS effect corresponds to the tension-resistance enhancement of interlayers due to the adhesion of glass fragments, which is beneficial for the post-fracture behavior of laminated glass. Nonetheless, it is worth noting that existing analytical models are based on the aligned crack pattern between two layers of fractured glass at room temperature. There is still much work to be done for investigating the TS effect in-depth and developing more precisely analytical model in the PFLS considering close-to-reality crack pattern and different service temperatures.

The crack pattern affects the TS effect by changing stress trajectories, whilst the temperature influences the TS effect due to the thermal dependency of the interlayer (Xie et al., 2024) and the interfacial property (Tian et al., 2012; Yang et al., 2022). The case with aligned cracks is usually considered to analyze the post-fracture capacity of laminated glass out of its assumed simplicity and engineering application. Angelides et al. (2021) experimentally investigated the out-of-plane bending moment capacity of aligned-crack laminated glass at different temperatures. However, offset crack patterns are getting more attention because of the mechanical enhancement originated from tension stiffening addressed in experimental (Biolzi et al., 2016; Biolzi et al., 2018) and numerical (Baraldi et al., 2016) investigations. The works considering more complicated crack patterns have been gaining focus. Nhamoinesu and Overend (2010) pioneered the offset-crack tension (OCT) tests for considering close-to-reality crack geometries. Biolzi et al. (2016) took into account the realistic crack morphology based on the “material specimens” cut from fractured laminated glass. Samieian et al. (2018) investigated the tensile response of laminated glass with random cracks, which were created by a ball hammer. Wang et al. (2022) developed a microscale discrete element model for investigating the influence of crack aligning, fragment size, and adhesion conditions. The authors generalized about the gradual diminishing of tension stiffening with fragment size decreasing. However, the investigation about the influence of crack patterns on the TS effect in conjunction with temperatures is nearly limited, which should be elaborately conducted further.

Besides, the delamination also contributes to a considerable change in terms of mechanical properties of laminated glass. Dural and Oyar (2023) pointed the evident influence of the delamination size and location on intact laminated glass. Biolzi et al. (2016) analyzed the stiffness increment of the interlayer due to the TS effect considering different delamination ratios. The stiffness of the interlayer for the crack pattern with maximum offset exceeds three times compared with that of a symmetric crack layout when the delamination ratio is nearly 15%. Moreover, Fourton et al. (2020) pointed initial delamination length of nearly tens to a few hundred microns in the vicinity of pre-cracks for through-cracked tensile (TCT) specimens. Biolzi et al. (2016) observed the small initial debonding of fractured

tempered laminated glass with SentryGlas® (SG) using a photographic follow-up. Therefore, it is of key importance to consider the delamination in the TS effect analysis of the post-fracture laminated glass.

This paper is the preliminary work of the development of more precisely analytical models in the PFLS. The main aim is to elaborate the mechanical enhancement of tension stiffening considering different fragment overlaps and temperatures based on pre-crack tension experiments, including multiple through-cracked tensile (MTCT) tests with aligned crack and multiple offset-cracked tensile (MOCT) tests with maximum crack offset. Besides, the influence of more diverse fragment overlaps and initial delamination on the initial stiffness of fractured laminated glass due to the TS effect was explored according to developed finite element models.

2. Methodology

2.1. Experimental scheme

The laminated specimens were provided by Henan Zhongbo Glass Co., LTD, which were autoclaved at the constant temperature of 130°C and constant pressure of 1.1 MPa for 100 minutes. The specimen consists of two layers of float glass with polished edges and a layer of interlayers. The nominal length, width, and thickness of float glass are 240, 50, and 5 mm. PVB and SG both from Kuraray with a nominal thickness of 1.52 mm are Trosifol® UltraClear B200 NR and SentryGlas® Xtra™ SGR6000, respectively. The actual dimensions of laminated specimens were also measured before testing. Two types of crack setups were considered in MTCT and MOCT tests shown in Fig. 1, respectively. MTCT and MOCT corresponded to the lower and upper limits of the level of fragment overlaps in the TS effect. The fragment size was pre-defined as 30 mm long using the glass knife. The two individual fragments were designed in every glass ply of specimens. The scratches for producing pre-defined cracks were aligned in two glass layers for the MTCT, while the fragments of the lower glass layers were offset by half the size of the fragment for the MOCT. Besides, an aluminium sheet of 0.3 mm thickness was adhered to the specimens with the epoxy for providing sufficient friction between specimens and grippers.

The specimens were loaded under uniaxial tension using an electromechanical universal test machine with a load cell of 100 kN. The tests were conducted at 300 mm/min and approximate room temperature. However, three temperatures of specimens, 20, 50, and 80°C, were investigated. The specimens at 50 and 80°C were heated and stored in the environmental chamber for at least 24 hours, which makes sure that the specimens have been at specific temperatures. Then the specimen was taken out from the environmental chamber, gripped by grippers and loaded in the uniaxial direction, where the whole process was completed within 30 seconds for guaranteeing the slight decrease of specimen temperatures. In addition, the camera was fixed to capture the delamination and tearing of the polymeric interlayers shown in Fig. 2. Three identical specimens were considered to ensure the reliability of test results. The label of specimens was ruled as a form of crack setups (MTCT/MOCT), interlayer types (PVB/SG), testing temperatures (20/50/80), and identification number of specimens (1/2/3).

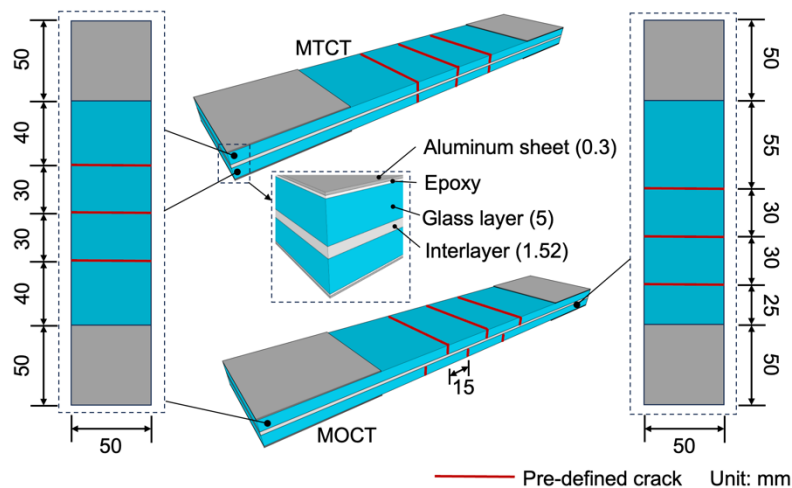


Fig. 1: Specimens of MTCT and MOCT tests.

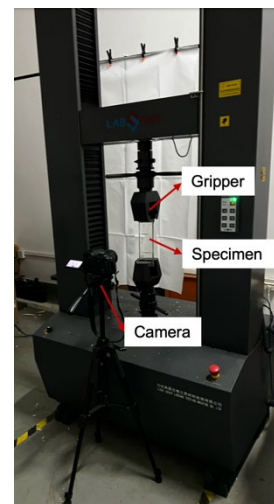


Fig. 2: Loading schematic.

2.2. Numerical model

The 2D numerical model developed in ABAQUS (2013) consists multiple glass fragments and a layer of the interlayer, considering different levels of the fragment offset and initial delamination. The representative model for MOCT is shown in Fig. 3. The geometries of the model correspond to those in the experiment. The fragment length a is 30 mm. The fragment overlap length s is 15mm. The length λ of initial delamination between pre-defined cracks is set as 0.1 mm according to the initial bridging interlayer ligament length of nearly tens to a few hundred microns pointed by Fourton et al. (2020). The glass thickness h and interlayer thickness t are 5 mm and 1.52 mm, respectively. The right end of the model is fixed, whilst the left is coupled with a reference point (RP), where the load is applied. Tie constraints are subjected to the glass/polymer interface at the bond regions. Besides, zero-thickness 4-node 2D cohesive elements (COH2D4) based on the cohesive zone model is applied in the pre-defined cracks and initial delamination zones. The interfacial stiffness, cohesive strength, and ultimate separation displacement in the cohesive zone model are set as 1 MPa/mm, 1×10^{-15} MPa, and 1×10^{-15} mm, respectively. The parameters in the cohesive zone model are sufficiently small, to not affect the mechanical properties of the numerical models and are suitable for the definition of pre-defined cracks and initial delamination.

A two-dimensional 4-node bilinear plane strain element with reduced integration and enhanced hourglass control (CPE4R) is used in the glass plies, whilst the hybrid formulation is added for interlayer elements (CPE4RH) considering that the Poisson's ratio of 0.49 exceeds 0.48 and convergence problems might emerge. The simulation in this paper only involves small deformations out of the difficulty of the nonlinearity and fracture of interlayers under large deformation in numerical models. Therefore, the model is tensioned by 0.5 mm for PVB and 0.25 mm for SG considering that the specimens did not experience delamination and tearing of interlayers under a specific stretch according to experimental observations, which is elaborated in Section 3.1 and 3.3 in detail. The glass and interlayer use elastic and viscoelastic models, where the detailed parameters are presented in Table 1. Considering the dependence of interlayers on the strain rate and the small initial delamination between pre-defined cracks, the viscoelastic constitutive model is more suitable compared with the elastic and hyperelastic models out of the varying strain rate. Besides, the actual loading displacement of the experiments versus time is considered in the numerical model shown in

Fig. 4, which is obtained by the fixed camera. The specimens made with PVB and at 20°C are used to determine the regular loading procedure of testing machine. The average loading curve is taken into account finally.

Table 1: Detailed parameters used in the numerical model.

Material	Density (kg/m ³)	Poisson's ratio	Constitutive model
Glass	2500 (Galuppi and Royer-Carfagni, 2023)	0.23 (Grozdanic et al., 2023)	Elastic model (70000 MPa (Grozdanic et al., 2023))
PVB	1100 (Wang et al., 2018)	0.49 (Wang et al., 2018)	Viscoelastic model (Xie et al., 2024)
SG	1100 (Bedon and Louter, 2014)	0.49 (Bedon and Louter, 2014)	Viscoelastic model (Xie et al., 2024)

The analysis of the mesh sensitivity made with PVB and initial delamination of 0.1 mm in Fig. 3 was conducted. Four types of the global mesh size, including 0.2, 0.1, 0.05, and 0.02 mm, were used. The calculation was implemented using the dynamic implicit solver based on the processor of 3.00 GHz 13th Gen Intel® Core™ i9-13900KF with the acceleration of NVIDIA GeForce RTX 3060 GPU. The ultimate force and computational time are presented in Fig. 5. The computational time intensely increases for the mesh size of 0.02 mm, while there is a slight variation of the ultimate force. Therefore, the global mesh size of 0.05 mm is finally chosen in the combination of computational accuracy and efficiency, which is close to the studies realised by Chen et al. (2023).

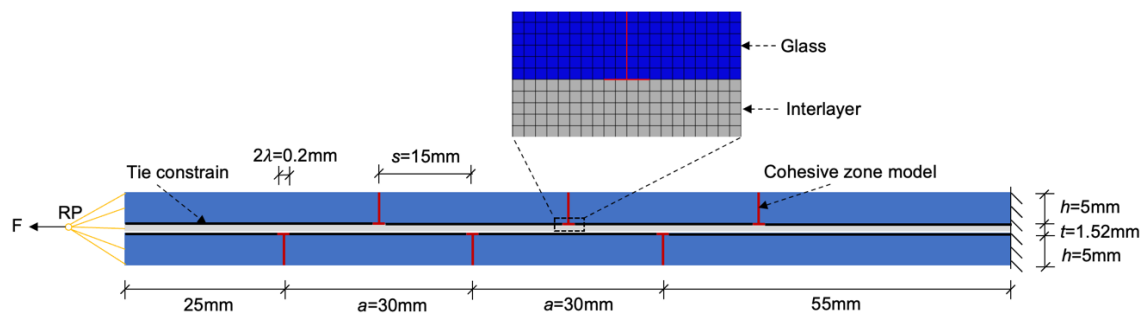


Fig. 3: Representative numerical model for MOCT.

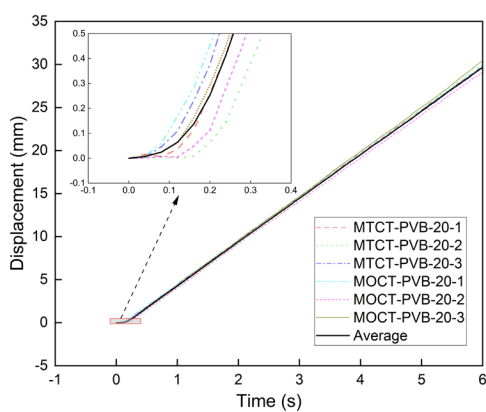


Fig. 4: Loading displacement.

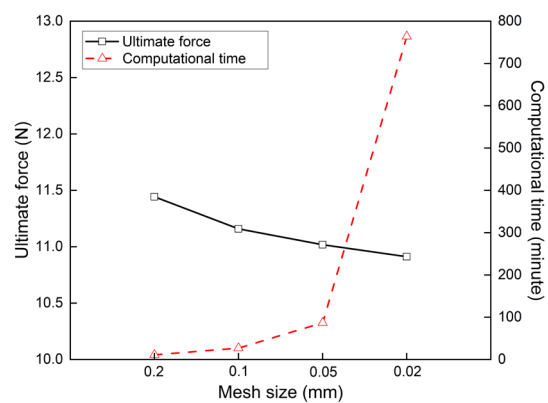


Fig. 5: Mesh convergence analysis.

3. Experimental results and discussions

3.1. Force-displacement curves

The force-displacement curves of MTCT and MOCT tests for PVB-laminated specimens are shown in Fig. 6. The evident differences can be seen in Fig. 6 (a, b, c) between MTCT and MOCT tests at three types of temperatures. There are dramatic peaks in the force-displacement curves for MOCT tests in Fig. 6, which significantly exceeded the maximum forces for MTCT tests. This means that the fractured laminated glass with offset cracks could provide higher tensile strength compared with the through-cracked case. The results of SG-laminated specimens are presented in Fig. 7. The specimens with offset cracks exhibit higher force-resistance than those with aligned cracks. Besides, it is clear from Fig. 7 that the stiffness decreasing of SG with increasing temperatures delays the advent of force-resistance peak.

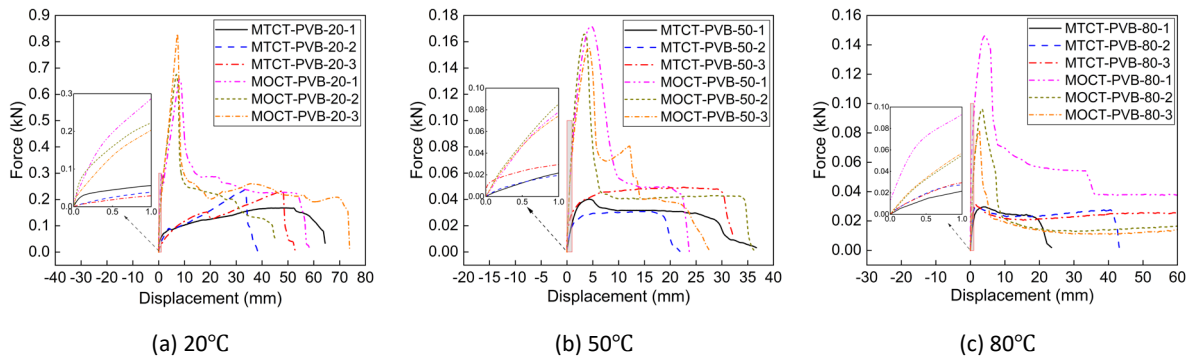


Fig. 6: Experimental results for PVB-laminated specimens.

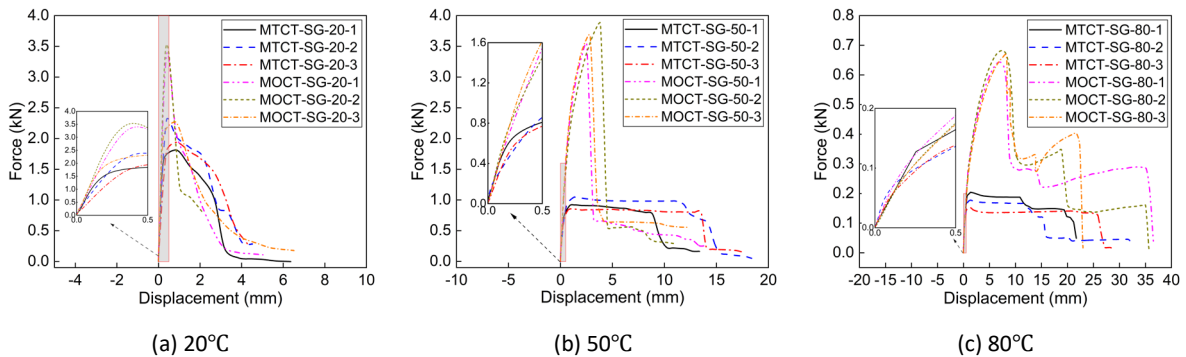


Fig. 7: Experimental results for SG-laminated specimens.

3.2. Failure modes

The stretching of PVB and an interfacial delamination could be found during the procedure of MTCT tests, ending up with the tearing of the PVB (shown in Fig. 8). When the interface starts to delaminate in MOCT tests, decreasing of bonding area weakens the tension stiffening. The reaction force decreases with increasing delamination area. Besides, more delamination is observed in MOCT tests, which is caused by more forces transferred from the PVB to the glass than that in MTCT tests. Therefore, glass fragments presented a rotation in MOCT tests due to less bonding with PVB shown in Fig. 8.

Due to the excellent adhesion of SG with glass, no delamination could be found in experiments at 20 (shown in Fig. 9) and 50°C. These specimens in MTCT tests fail by tearing of SG, along with the slight stretching of SG. However, the glass fracture in MOCT tests at 20 and 50°C locates in the middle of pre-

defined glass fragment in one glass ply and aligns with pre-defined crack in another glass ply. The high shear transference derived from the strong adhesion of SG leads to the high tensile stress in the glass layers. However, the temperature finally presents a remarkable influence on the performance of SG specimens at 80°C, where the interfacial delamination and tearing of SG contribute to the failure. The interfacial properties have been weakened at 80°C for laminates with SG.

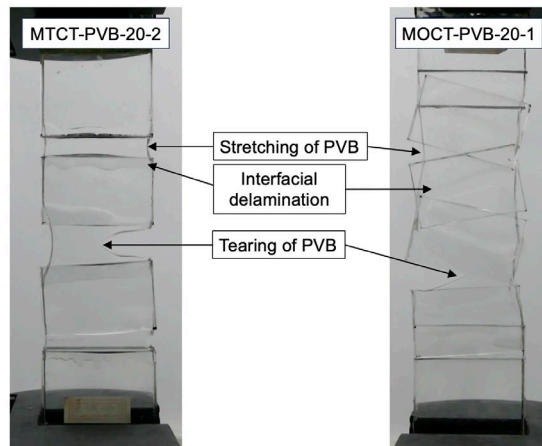


Fig. 8: Interfacial delamination, tension, and tearing of PVB in MTCT and MOCT tests.

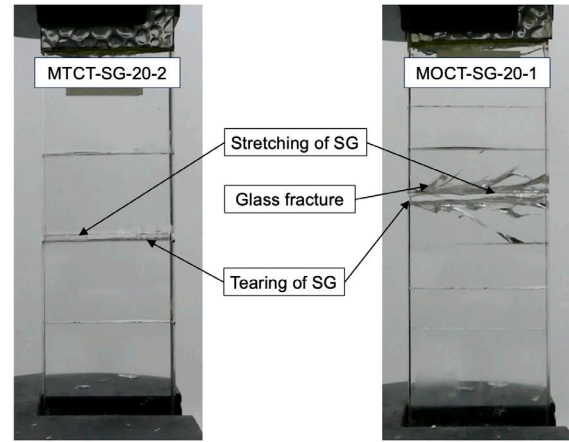


Fig. 9: Glass fracture, tension and tearing of SG in MTCT and MOCT tests.

3.3. Initial stiffness and strength

The initial stiffness k_{eqi} and strength σ_s of equivalent materials for the pre-defined specimens were calculated according to Eq.(1) and Eq.(2). The initial stiffness of PVB specimens is determined as the secant modulus at 0.5 mm, where slight nonlinearity is presented in Fig. 6 and no obvious delamination occurs in the light of experimental observations. The results of the initial stiffness and strength of equivalent materials made with PVB are presented in Fig. 10. The mechanical enhancement of the TS effect decreases with increasing temperatures in the case of the initial stiffness and strength in Fig. 10 (a) and (b). Besides, the improvement of the strength (254-309%) is consistently higher than that for the initial stiffness (168-187%) at 50 and 80°C.

$$k_{eqi} = \frac{F_d L}{dtb} \quad (1)$$

$$\sigma_s = \frac{F_{max}}{tb} \quad (2)$$

Where F_d denotes the force at loading displacement d , F_{max} denotes the maximum force in force-displacement curves, t is the nominal thickness of interlayer, L and b are the length and width of specimens, respectively.

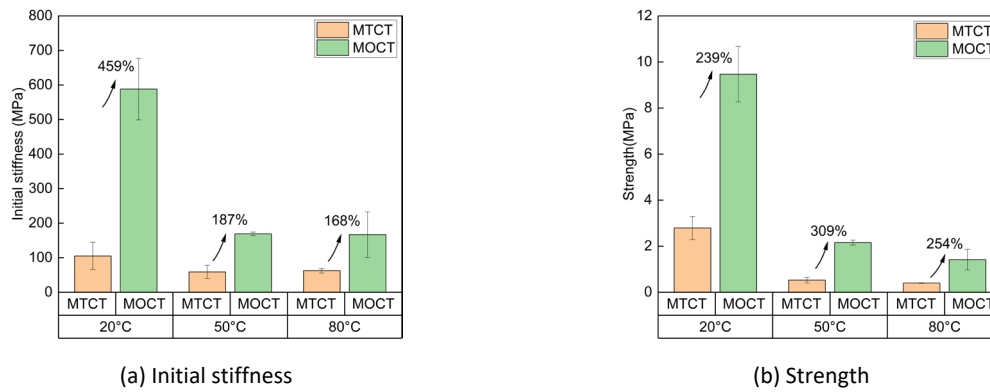


Fig. 10: Initial stiffness and strength of equivalent materials made with PVB.

Although the curves nearly have a linear ascending within loading displacement of 0.5 mm at 50 and 80°C in Fig. 7 (b) and (c), the displacement corresponding to the peak of force-displacement curves in MOCT tests is below 0.5 mm in Fig. 7 (a). Therefore, 0.25 mm is chosen for determining the initial stiffness of equivalent materials made with SG. The influences of temperatures on the initial stiffness and strength enhancement for SG-laminated specimens present a considerable difference from those of PVB-laminated specimens. The temperature affects the equivalent initial stiffness of SG-laminated specimens less significantly compared with that of PVB-laminated specimens. At 80°C, there is rarely a distinction for the initial stiffness between MTCT and MOCT tests. However, an obvious deviance can be found where the SG-laminated equivalent strength at 50°C is higher compared with that at 20°C for MOCT tests shown in Fig. 11 (b). It might be related to the glass transition temperature of SG and the temperature dependence of the interface.

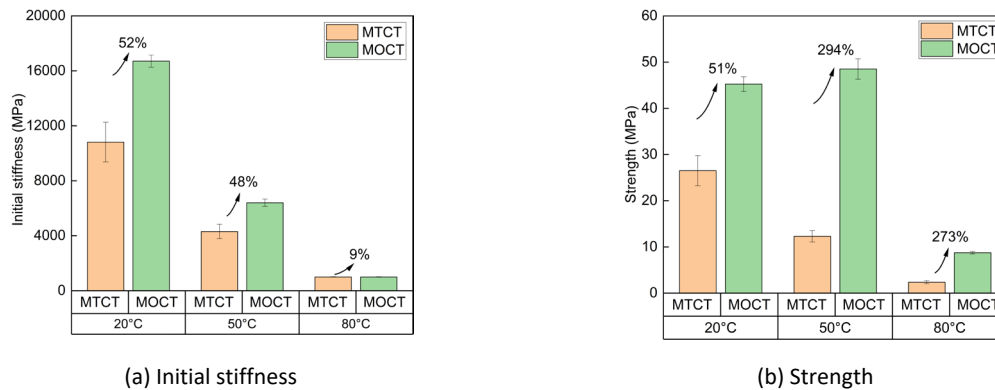


Fig. 11: Initial stiffness and strength of equivalent materials made with SG.

The mechanical enhancement due to the TS effect generally presents a more evident tendency with interlayer stiffness decreasing at higher temperatures. However, the high temperature weakens the interfacial adhesion, which restricts the stress transfer and contribution of the TS effect. Accordingly, competitive mechanism contributing to the TS effect with temperature changing exists in fractured laminated glass. More researches are planned to be conducted at different temperatures for describing its influence on the TS effect in detail.

4. Parametric study

Due to the limitation of experiments, more cases for different fragment overlaps and delamination lengths, that are important to the TS effect, are studied based on the developed finite element models. The lower and upper limits of fragment overlaps have been investigated in experiments. In this section, the variants including dimensionless fragment overlap rate ζ (Eq. (3)) and initial delamination length λ are chosen, while the other parameters are consistent with those in experiments. Temperatures of 20°C are considered in the numerical simulation. The equivalent initial stiffness k_{eqi} according to Eq. (1) is extracted to investigate the influence of the fragment overlap and initial delamination on k_{eqi} . The range of $0 \sim 1$ is considered for ζ , while 0.1, 0.5, and 1 mm are chosen for λ .

The results from finite element models are presented in Fig. 12. It is clear from Fig. 12 that “swoosh-shaped” nonlinearity regulates the influence of the fragment overlap rate on the initial stiffness. The initial stiffness reaches its lowest point at around $\zeta = 0.1$, which means that the pattern of aligned cracks rarely corresponds to the worst mechanical properties, at least not for the equivalent initial stiffness. Besides, the increasing of initial delamination length has a negative effect on the initial stiffness. In comparison with results from simulations, results from experiments (MTCT tests correspond to $\zeta = 0$, while $\zeta = 1$ for MOCT tests) are lower, excluding the case of SG-laminated specimens in MTCT tests. It can be directly estimated from Fig. 12 that specimens in experiments should have an initial delamination length of above 1.0 mm. But something should be clarified that there is no visible initial delamination observed in specimens before experiments. If the initial delamination length exceeds 1.0 mm, it can be observed by naked eyes. Probable reasons that the results from the models are higher than those from the experiments encompass the assumption of the perfect bonding interface and the usage of nominal thicknesses in models. Further studies will be conducted.

$$\zeta = \frac{2s}{a} \quad (3)$$

Where s is the fragment overlap length, a is the fragment length.

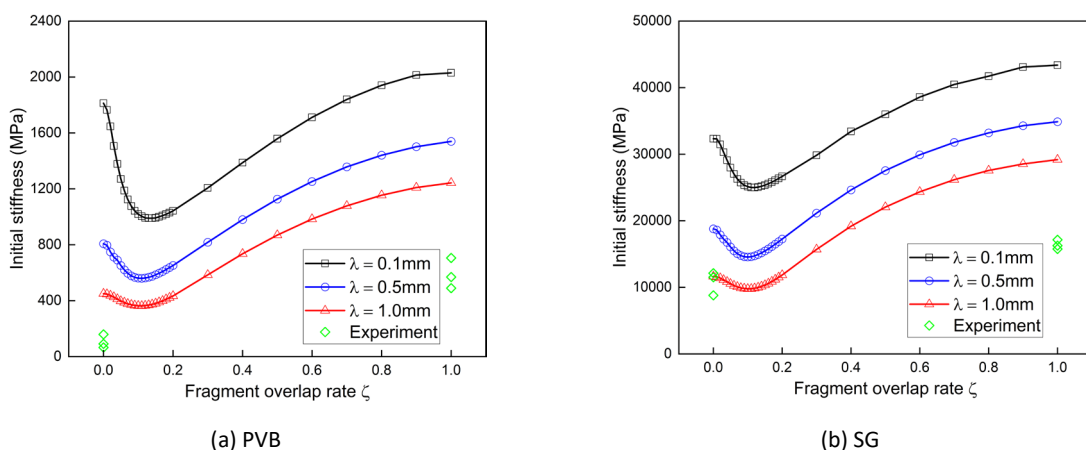


Fig. 12: Initial stiffness at 20°C by finite element models.

For clarifying the mechanics of the nonlinearity in Fig. 12, the stress contour plots at different fragment overlap rates have been presented in Fig. 13 based on the case of PVB-laminated models with 0.1 mm initial delamination. The normal stress in the x direction (s_{11}) that adheres to the direction of loading tension is focused on. When the fragment overlap rate is relatively small ($\zeta < 0.1$), the force flows mainly through the connectivity interlayer between adjacent cracks. The mechanical mode changes gradually from the tension in the interlayers to the shear, which makes the initial stiffness of equivalent materials decrease as ζ increases. For $\zeta > 0.15$, the adjacent cracks are so far that the force is prone to be transferred through the glass rather than the connectivity interlayer. In this case, the TS effect gets more evident along with larger fragment overlap rates due to more force being transferred into the glass. Therefore, a nonlinear influence of the fragment overlap on the initial stiffness is presented Fig. 12.

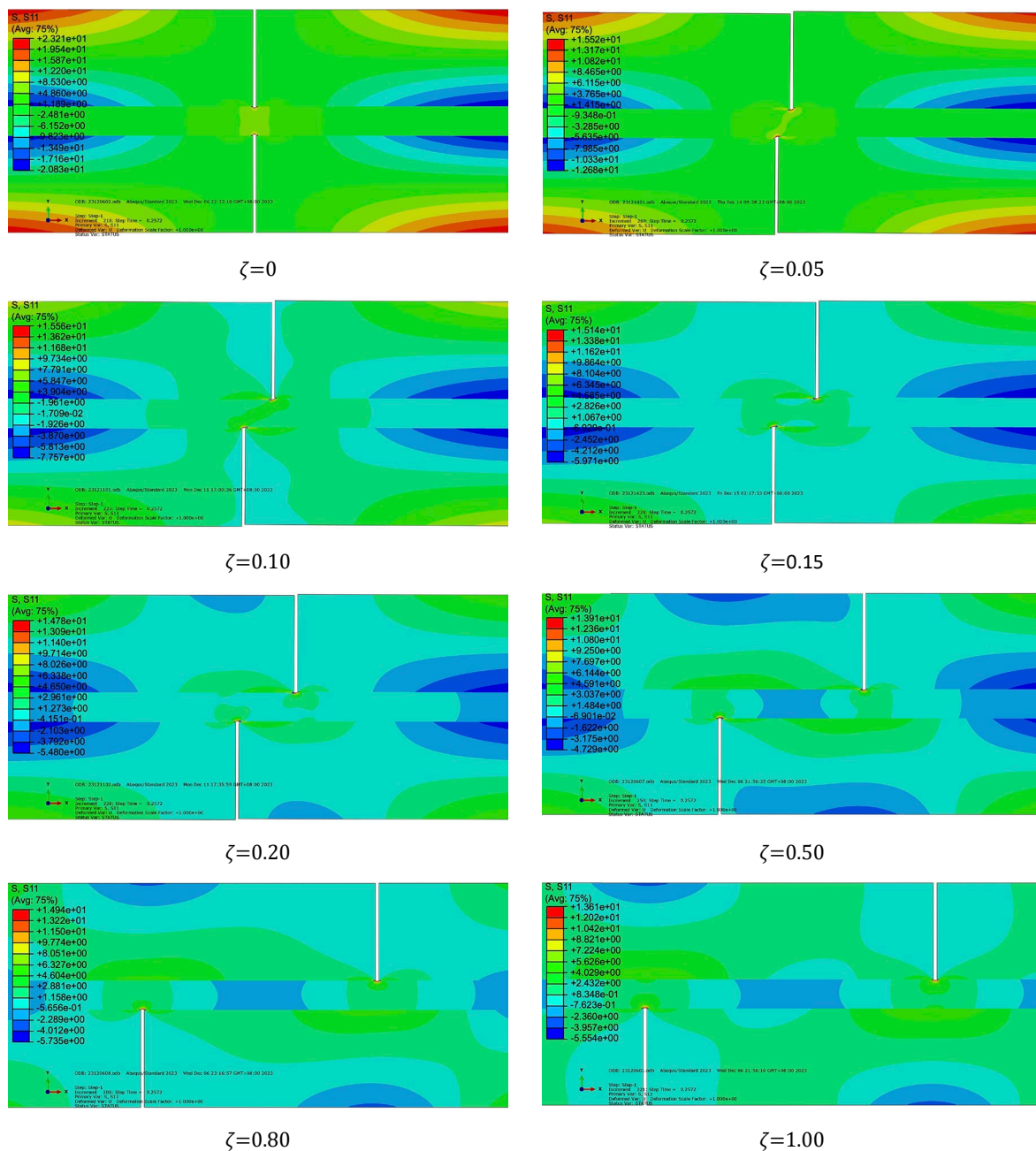


Fig. 13: Stress contour plot at different fragment overlap rates.

5. Conclusion

This paper aims to provide rudimentary research on the tension stiffening (TS) effect. Multiple though-cracked tensile tests and multiple offset-cracked tensile tests at 20, 50, and 80°C were conducted for investigating the influence of the fragment overlap and temperature. Besides, finite element models were developed for exploring the influence of diverse fragment overlaps and initial delamination on the initial stiffness of fractured laminated glass. The results indicate that the fragment overlap and temperature should be considered carefully in the Post Fracture Limit State (PFLS) due to the TS effect. Also, a complex influence of the fragment overlap on the equivalent initial stiffness emerges, where the mechanism has been elaborated based on finite element models. More investigations should be conducted on the equivalent strength for developing precisely analytical models in the PFLS. The influence of the strain rate on the TS effect should be included as well.

Acknowledgements

This study was funded by the National Natural Science Foundation of China [grant no. 52078293]. The authors thank the Henan Zhongbo Glass Co., Ltd. for supplying testing materials.

References

- Abaqus 6.13 Analysis user guide, Dassault Syst`emes, Providence, RI, USA (2013).
- Angelides, S.C., Talbot, J.P., Overend, M.: High strain-rate effects from blast loads on laminated glass: An experimental investigation of the post-fracture bending moment capacity based on time–temperature mapping of interlayer yield stress. *Construction and Building Materials* 273, 121658 (2021). <https://doi.org/10.1016/j.conbuildmat.2020.121658>
- Baraldi, D., Cecchi, A., Foraboschi, P.: Broken tempered laminated glass: Non-linear discrete element modeling. *Composite Structures* 140, 278–295 (2016). <https://doi.org/10.1016/j.compstruct.2015.12.050>
- Bedon, C., Louter, C.: Exploratory numerical analysis of SG-laminated reinforced glass beam experiments. *Engineering Structures* 75, 457–468 (2014). <https://doi.org/10.1016/j.engstruct.2014.06.022>
- Biolzi, L., Cattaneo, S., Orlando, M., Piscitelli, L.R., Spinelli, P.: Post-failure behavior of laminated glass beams using different interlayers. *Composite Structures* 202, 578–589 (2018). <https://doi.org/10.1016/j.compstruct.2018.03.009>
- Biolzi, L., Orlando, M., Piscitelli, L.R., Spinelli, P.: Static and dynamic response of progressively damaged ionoplast laminated glass beams. *Composite Structures* 157, 337–347 (2016). <https://doi.org/10.1016/j.compstruct.2016.09.004>
- Biolzi, L., Simoncelli, M.: Overall response of 2-ply laminated glass plates under out-of-plane loading. *Engineering Structures* 256, 113967 (2022). <https://doi.org/10.1016/j.engstruct.2022.113967>
- Chen, X., Lin, B., Schuster, M., Chen, S., Xu, B.-X., Schneider, J.: Effect of moisture on the delamination properties of fractured PVB-laminated glass: A joint experimental and numerical study. *Composite Structures* 322, 117381 (2023). <https://doi.org/10.1016/j.compstruct.2023.117381>
- D'Ambrosio, G., Galuppi, L., Royer-Carfagni, G.: A simple model for the post-breakage response of laminated glass under in-plane loading. *Composite Structures* 230, 111426 (2019). <https://doi.org/10.1016/j.compstruct.2019.111426>
- Dural, E., Oyar, F.: Effect of delamination size, location and boundary conditions on the behavior of a laminated glass plate. *Structures* 47, 121–133 (2023). <https://doi.org/10.1016/j.istruc.2022.11.034>
- Feldmann, M., Laurs, M., Belis, J., Buljan, N., Criaud, A., Dupont, E., Eliasova, M., Galuppi, L., Hassinen, P., Kasper, R., Louter, C., Manara, G., Minne, A., Morgan, T., Pisano, G., Overend, M., Royer-Carfagni, G., Schneider, J., Schwind, G., Schuler, C., Siebert, G., Sikynova, A.: The new CEN/TS 19100: Design of glass structures. *Glass Struct Eng* 8, 317–337 (2023). <https://doi.org/10.1007/s40940-023-00219-y>
- Fourton, P., Piroird, K., Ciccotti, M., Barthel, E.: Adhesion rupture in laminated glass: influence of adhesion on the energy dissipation mechanisms. *Glass Struct Eng* 5, 397–410 (2020). <https://doi.org/10.1007/s40940-020-00136-4>
- Galuppi, L., Amadio, C., Badalassi, M., Bedon, C., Biolzi, L., Briccoli Bati, S., Cagnacci, E., Consolini, L., Cuomo, M., Dall'Igna, R., D'Este, A., Faggiano, B., Fagone, M., Foraboschi, P., Franco, A., Lani, L., Maceri, F., Manara, G., Mognato, E., Spinelli, P.:

CNR DT210/2013 Istruzioni per la Progettazione, l'Esecuzione ed il Controllo di Costruzioni con Elementi Strutturali di Vetro (2013).

- Galuppi, L., Royer-Carfagni, G.: A homogenized model for the post-breakage tensile behavior of laminated glass. *Compos. Struct.* 154, 600–615 (2016). <https://doi.org/10.1016/j.compstruct.2016.07.052>
- Galuppi, L., Royer-Carfagni, G.: Thermal analysis of architectural glazing in uneven conditions based on Biot's variational principle: Part II—validation and case-studies. *Glass Struct Eng* 8, 57–80 (2023). <https://doi.org/10.1007/s40940-023-00217-0>
- Grozdanic, G., Ibrahimbegovic, A., Galic, M., Divic, V.: Multiscale beam model for simulating fracture in laminated glass structures. *Engineering Fracture Mechanics* 292, 109606 (2023). <https://doi.org/10.1016/j.engfracmech.2023.109606>
- Nhamoinesu, S., Overend, M.: Simple models for predicting the post-fracture behaviour of laminated glass, in: *Proceedings of the XXV ATIV 2010 International Conference*, Parma (2010).
- Samieian, M.A., Cormie, D., Smith, D., Wholey, W., Blackman, B.R.K., Dear, J.P., Hooper, P.A.: Temperature effects on laminated glass at high rate. *International Journal of Impact Engineering* 111, 177–186 (2018). <https://doi.org/10.1016/j.ijimpeng.2017.09.001>
- Thomas, W., Thiemo, F., Andreas, L.: New Swiss technical specification SIA 2057 for glass structures and its post failure limit state concept. *Glass Struct Eng* 8, 339–351 (2023). <https://doi.org/10.1007/s40940-023-00227-y>
- Tian, Y., Bao, Y.W., Wan, D.T., Wang, X.F., Han, Z.M.: Effect of Temperature on the Interfacial Bonding Strength between PVB and Glass from RT to -50 °C. *KEM* 492, 61–65 (2012). <https://doi.org/10.4028/www.scientific.net/KEM.492.61>
- Wang, X., Yang, J., Peng, S., Wang, Y., Hou, X.: Microscale Discrete Element Model for Simulating Bridging Behavior of Fractured Glass Laminates, in: *Challenging Glass Conference Proceedings* (2022). <https://doi.org/10.47982/cgc.8.451>
- Wang, X., Yang, J., Wang, F., Liu, Q., Xu, H.: Simulating the impact damage of laminated glass considering mixed mode delamination using FEM/DEM. *Composite Structures* 202, 1239–1252 (2018). <https://doi.org/10.1016/j.compstruct.2018.05.127>
- Wang, X.-E., Yang, J., Huang, X., Wang, F., Zhu, Y.: Voronoi-FDEM concept for modelling post-fracture response of progressively damaged structural glass. *Engineering with Computers* 38, 3025–3038 (2021). <https://doi.org/10.1007/s00366-021-01318-6>
- Xie, D., Yang, J., Zhao, C., Wang, X.: Comprehensive investigation into the thermal rheological behavior and relaxation characteristic of single/composite polymers in laminated glass. *Thin-Walled Structures* 195, 111369 (2024). <https://doi.org/10.1016/j.tws.2023.111369>
- Yang, J., Wang, Y., Wang, X., Hou, X., Zhao, C., Ye, J.: Local bridging effect of fractured laminated glass with EVA based hybrid interlayers under weathering actions. *Construction and Building Materials* 314, 125595 (2022). <https://doi.org/10.1016/j.conbuildmat.2021.125595>

Platinum Sponsor



Gold Sponsors



Silver Sponsors



Organising Partners

